Science of the Total Environment 627 (2018) 1253–1263

Contents lists available at ScienceDirect

Science of the Total Environment

journal homepage: www.elsevier.com/locate/scitotenv

Nanomaterials for treating emerging contaminants in water by adsorption and photocatalysis: Systematic review and bibliometric analysis

Lin Zhao [a,1], Jinghui Deng [a,1], Peizhe Sun [a], Jiashu Liu [a], Yi Ji [a], Norihide Nakada [b], Zhi Qiao [a], Hiroaki Tanaka [b], Yongkui Yang [a,*]

[a] School of Environmental Science and Engineering, Tianjin University, Tianjin 300072, China
[b] Research Center for Environmental Quality Management, Graduate School of Engineering, Kyoto University, 1-2 Yumihama, Otsu, Shiga 520-0811, Japan

HIGHLIGHTS

- A review of nanomaterials for emerging pollutant removal from water.
- Literature related to adsorption and photo-catalysis is reviewed.
- Large-scale bibliometric analysis of papers published in 1998–2017.
- General research trends and future directions are discussed.

GRAPHICAL ABSTRACT

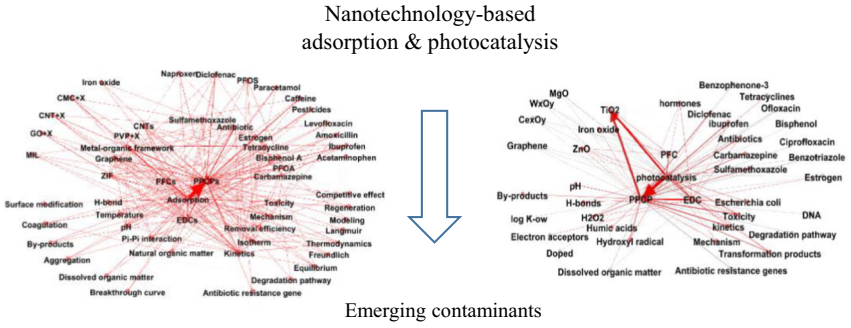

ARTICLE INFO

Article history:
Received 8 January 2018
Received in revised form 1 February 2018
Accepted 1 February 2018
Available online 7 February 2018

Editor: D. Barcelo

Keywords:
Emerging contaminants
Nano
Adsorption
Photocatalysis
Bibliometrics

ABSTRACT

Emerging contaminants in the aquatic environment have become a worldwide problem. Conventional wastewater treatment processes are ineffective for eliminating the emerging contaminants at trace concentrations. Nanomaterials possessing novel size-dependent properties, however, have shown great potential for removing these contaminants. Herein we reviewed nanomaterials reported for removing emerging contaminants by adsorption and/or photocatalysis, and their removal capacity, mechanism, and influencing factors are discussed. Meanwhile, a large-scale bibliometric analysis is conducted on the trends of the emerging contaminants, nanoadsorbents, nanophotocatalysts, and related research topics from the literature during 1998–2017.

Abbreviations: 3D GT, three-dimensional macrostructure; ATN, atenolol; ACT, acetaminophen; AML, amiloride; CA, clofibric acid; CMC, carboxy methyl cellulose; CMC-FMBO, carboxymethyl cellulose binary oxide Fe-Mn nanoparticle; CNT, carbon nanotube; DCF, diclofenac; E2, 17β-estradiol; EE2, 17α-ethinylestradiol; EDC, endocrine disrupting chemical; GAC, granular activated carbon; GO, graphene oxide; IBP, ibuprofen; LEV, levofloxacin; MIL, chromium (III) terephthalate; MIL-101(Cr)/SA, MIL-101/sodium alginate; MIL-101(Cr)/CS, MIL-101/chitosan; MWCNT, multiwall carbon nanotube; NPX, naproxen; NM, anti-inflammatory nimesulide; NP, nanoparticle; OCBA, other carbon-based adsorbent; OMOF, other metal-organic framework; PFC, perfluorinated compound; PFOA, perfluorooctanoic acid; PFOS, perfluorooctane sulfonate; PPCP, pharmaceuticals and personal care product; PVP, polyvinylpyrrolidone; SCI, science citation index; SWCNT, single-wall carbon nanotube; TMP, trimethoprim; ZIF, zeolitic imidazole framework; ZIF–GO, zeolitic imidazole frameworks-graphene oxide.

* Corresponding author.
E-mail address: ykyang@tju.edu.cn (Y. Yang).
[1] These authors contributed equally to this work.

https://doi.org/10.1016/j.scitotenv.2018.02.006
0048-9697/

1. Introduction

In the last few decades, the existence of emerging contaminants in the aquatic environment has become a worldwide issue. These emerging contaminants include pharmaceuticals and personal care products (PPCPs), endocrine disrupting chemicals (EDCs), perfluorinated compounds (PFCs), etc. They are commonly present at concentrations of mg/L to ng/L in wastewater (Alder et al., 2010; Behera et al., 2011), surface water (Kleywegt et al., 2011; Peng et al., 2008), ground water (Loos et al., 2010; Maeng et al., 2010), and drinking water (Benotti et al., 2009; Stackelberg et al., 2004), posing great risks to human health and natural ecosystems due to their short- and long-term toxicities (Ratola et al., 2012; Richardson and Ternes, 2011).

Current treatment technologies for emerging contaminants include the conventional activated sludge-based biological system, adsorption by activated carbon, membrane filtration, and chemical treatments (chlorination, ozonation, UV irradiation, and permanganate oxidation). However, occasionally these conventional processes fail to sufficiently remove the emerging contaminants to the levels required by discharge standard or essential for the wastewater reuse (Castiglioni et al., 2006; Heberer, 2002; Rivera-Utrilla et al., 2013). Therefore, new treatment technologies and infrastructures are needed to provide high-quality water for human and environmental needs. Recent advances in nanotechnology have offered ample opportunities to develop next-generation water treatment processes. Compared with traditional materials in the forms of bulk or large particles, some nanomaterials have shown better potential in removing emerging contaminants in lab-scale studies, owing to their unique size-dependent properties. These materials often display high specific surface area, high surface free energy, sufficient reactive sites, fast dissolution, and various discontinuous properties (e.g. superparamagnetism, localized surface plasmon resonance, and quantum confinement effect) (Qu et al., 2013). Many nanotechnology studies are centered on the adsorption, photocatalysis, membrane filtration, monitoring, disinfection and microbial control in treating water and wastewater. Especially, adsorption and photocatalysis by nanomaterials have been extensively studied for potential applications. The adsorption process has the advantage of efficient pollutant removal from aqueous phase. On the other hand, photocatalysis can not only remove the chemically stable and non-biodegradable organic pollutants, but also efficiently degrade trace organic pollutants under mild conditions, yielding minimal by-products. Therefore, adsorption and photocatalysis are considered very promising technologies in water treatment.

However, despite many studies in the past few years on nanoadsorption and nanophotocatalysis for the removal of emerging contaminants, their practical applications remain limited. To further focus the directions of related research and help solve key scientific problems towards practical applications, here we present a systematic review and bibliometric analysis on the application of nanotechnology to adsorption and photocatalysis for treating emerging contaminants in water. This study comprehensively examines the current status and the future of this research field through detailed review and large-scale bibliometric analysis.

2. Adsorption process

In general, the adsorption of emerging contaminants on the surface of carbon-based (Kumar and Mohan, 2012; Zhao et al., 2016) and metal-organic framework (MOF)-based nanomaterials (Song and Jhung, 2017; Shan and Tong, 2013; Yean et al., 2005) is mainly determined by the physical structure and chemical properties of the materials, as the specific surface area, pore structure, and surface functional groups may directly affect the adsorption capacity.

2.1. Carbon-based nanoadsorbents

2.1.1. Adsorption capacity

Carbon-based nanoadsorbents are the most widely used type of adsorbents for water treatment. The reported adsorption capacity data are summarized in Table 1. The adsorption strongly depends on the type of emerging pollutant as well as the nanoadsorbents. The removal of sulfapyridine, ciprofloxacin, and tetracycline by carbon nanotubes (CNTs) has been studied in water environments (Apul and Karanfil, 2015). About 90% of lincomycin and sulfamethoxazole (both 12,000 mg/L) were removed via adsorption on single-wall carbon nanotubes (SWCNTs) and multiwall carbon nanotubes (MWCNTs) (Kim et al., 2014). The maximum adsorption capacity of CNTs for sulfapyridine in water at pH 7 was 86.1 mg/g, while that for sulfamethoxazole was 45.8 mg/g (Tian et al., 2013). About 50 mg of CNTs could remove 67.5% of ciprofloxacin at 30 mg/L in water at pH 5 (Carabineiro et al., 2012). Graphite and CNTs could achieve 92% tetracycline removal from water, and the adsorption coefficient (Kd) values of SWCNTs, MWCNTs, and graphite measured from single-point adsorption are almost 1500, 1100, and 120 L/kg, respectively (Ji et al., 2010a). The sorption data of tetracycline on MWCNTs could be well interpreted by the Langmuir model, with the maximum adsorption capacity being 269.5 mg/g and the removal rate being 99.8% (Zhang et al., 2011). Graphene oxide (GO) showed maximum adsorption capacities of 256.6 mg/g for levofloxacin (LEV) and 89.1 mg/g for metformin (Dong et al., 2016; S. Zhu et al., 2017). The Langmuir isotherm model also produced better fits to the equilibrium acetaminophen (ACT) adsorption, with the maximum adsorption capacity of 704 mg/g by double-oxidized GO (Moussavi et al., 2016). Three-dimensional macrostructures (3D GTs) by two-dimensional GO nanosheets and one-dimensional CNTs showed superior adsorption capabilities towards oxytetracycline (1729 mg/g) and diethyl phthalate (680 mg/g) (Shen et al., 2017). The reduced GO showed a maximum adsorption capacity of anti-inflammatory nimesulide (NM) of 82.4 mg/g at 25 °C (Jauris et al., 2017).

2.1.2. Adsorption mechanism

Carbon-based nanoadsorbents have strong affinity for polar organic compounds, mainly due to the diverse interactions of these adsorbates with the adsorbent, including hydrophobic effect, π-π interactions, hydrogen bonding, covalent bonding, and electrostatic interactions (Ersan et al., 2017).

2.1.2.1. π-π interaction. The π–π interaction between compounds that accept π electrons and the π electron-rich regions of the grapheme surface of CNTs and graphite was observed during triclosan adsorption (Ji et al., 2010b; Liu et al., 2012). A similar mechanism was reported for KOH-activated CNTs for the adsorption of sulfamethoxazole, tetracycline, and tyrosine (Chen et al., 2008; Ji et al., 2009). The π-π interaction was dominant for the adsorption of chemicals containing benzene rings (e.g. 17-ethinylestradiol and bisphenol A) on carbon nanomaterials (Chen et al., 2007). Triclosan contains two aromatic rings that are favored for π–π interaction with the graphene structure on the CNT surface. In comparison, ibuprofen (IBP) contains only one aromatic ring in its molecular structure, resulting in weaker π–π interaction with the CNTs (Wang et al., 2015). Using computer simulations, the adsorption of NM onto GO was found to be maintained primarily by π–π type interactions (Jauris et al., 2017). For LEV, both π–π and electrostatic interactions govern the sorption onto GO-based adsorbents (Dong et al., 2016).

2.1.2.2. Electrostatic interactions. When the solution pH is different from the isoelectric point (pH_{pzc}) of carbon-based nanoadsorbents, the surface of the nanoadsorbent will carry either positive or negative charge. At the same time, ionizable emerging contaminants can also be protonated or deprotonated and become charged at different pH. For example,

Table 1
Adsorption of the emerging contaminants on various nanomaterials in water.

Nanomaterials		Pollutants	Maxmium adsorption (q_m, mg/g); adsorption coeffcient (k_F, $mmol^{1-n}\ L^n\ kg^{-1}$)	Treatment conditions	References
Carbon based	MWCNT	Triclosan	q_m 157.7	T 25 °C; pH 7	Zhou et al., 2013
	MWCNT	Norfloxacin	q_m 88.5	T 30 °C; pH 7	Yang et al., 2012
	MWCNT	Sulfamethoxazole	k_F 201	T 20 °C	Kim et al., 2014
	MWCNT	Lincomycin	k_F 287	T 20 °C	Kim et al., 2014
	MWCNT	Sulfamethoxazole	q_m 45.8	pH 7	Tian et al., 2013
	MWCNT	Sulfapyridine	q_m 86.1	pH 7	Tian et al., 2013
	MWCNT	Sulfapyridine	k_F 350	pH 6.2	Ji et al., 2009
	MWCNT	Sulfamethoxazole	k_F 510	pH 6.2	Ji et al., 2009
	MWCNT	Ciprofloxacin	q_m 135	T 25 °C; pH 5	Carabineiro et al., 2012
	MWCNT	Tetracycline	k_F 240	pH 5	Ji et al., 2010a, 2010b
	MWCNT	Tetracycline	q_m 269.5	T 20 °C	Zhang et al., 2011
	MWCNT	Sulfonamides	k_F 353–2814	T 25 °C	Zhao et al., 2016
	MWCNT	Chloramphenicols	k_F 571–618	T 25 °C	Zhao et al., 2016
	MWCNT	Non-antibiotic pharmaceuticals	k_F 317–1522	T 25 °C	Zhao et al., 2016
	KOH-activated MWCNT	Phenol	k_F 457	pH 6	Ji et al., 2010a, 2010b
	KOH-activated MWCNT	Nitrobenzene	k_F 1100	pH 6	Ji et al., 2010a, 2010b
	KOH-activated MWCNT	Sulfamethoxazole	k_F 2300	pH 6	Ji et al., 2010a, 2010b
	KOH-activated MWCNT	Tetracycline	k_F 800	pH 6	Ji et al., 2010a, 2010b
	KOH-activated MWCNT	Tylosin	k_F 650	pH 6	Ji et al., 2010a, 2010b
	SWCNT	Sulfamethoxazole	k_F 6380	T 20 °C	Kim et al., 2014
	SWCNT	Tetracycline	k_F 1150	pH 5	Ji et al., 2010a, 2010b
	SWCNT	Lincomycin	k_F 1030	T 20 °C	Kim et al., 2014
	KOH-activated SWCNT	Phenol	k_F 800	pH 6	Ji et al., 2010a, 2010b
	KOH-activated SWCNT	Nitrobenzene	k_F 1840	pH 6	Ji et al., 2010a, 2010b
	KOH-activated SWCNT	Sulfamethoxazole	k_F 5200	pH 6	Ji et al., 2010a, 2010b
	KOH-activated SWCNT	Tetracycline	k_F 1400	pH 6	Ji et al., 2010a, 2010b
	KOH-activated SWCNT	Tylosin	k_F 910	pH 6	Ji et al., 2010a, 2010b
	Graphite	Tetracycline	k_F 12.2	pH 5	Ji et al., 2010a, 2010b
	Graphene oxide	Levofloxacin	q_m 256.6	T 25 °C	Dong et al., 2016
	Graphene oxide	Acetaminophen	q_m 704	T 25 °C; pH 8	Moussavi et al., 2016
	Graphene oxide	metformin	k_F 47.1	T 30 °C; pH 6	S. Zhu et al., 2017
	Graphene oxide	Anti-inflammatory nimesulide	q_m 82.41	T 25 °C	Jauris et al., 2017
	Graphene oxide	17-α-ethinylestradiol	q_m 45	T 25 °C	Sun et al., 2017
		17-β-estradiol	q_m 48	T 25 °C	
	CNTs-Graphene oxide	oxytetracycline	q_m 173	T 25 °C	Shen et al., 2017
	g-C_3N_4-Graphene oxide	17-β-estradiol	q_m 144.4	T 25 °C	Kumar et al., 2017
		ciprofloxacin	q_m 1368	T 25 °C	
Metal-organic framework	Zeolitic imidazole framework–magnetic graphene oxide	Benzotriazole	q_m 300	T 40 °C	Andrew Lin and Der Lee, 2016
	Chromium(III) terephthalat– MIL 101	Dimetridazole	q_m 185	T 25 °C; pH 6.3	Seo et al., 2017
	Chromium(III) terephthalat– MIL 101	Metronidazole	q_m 188	T 25 °C; pH 6.3	Seo et al., 2017
	Chromium(III) terephthalat– MIL 101	Triclosan	q_m 112	T 25 °C; pH 7	Song and Jhung, 2017
	Chromium(III) terephthalat– MIL 101	Bisphenol A	q_m 97	T 25 °C; pH 7	Song and Jhung, 2017
	Chromium(III) terephthalat– MIL 101	Naproxen	q_m 156	T 25 °C; pH 7	Song and Jhung, 2017
	Chromium(III) terephthalat– MIL 101	Ketoprofen	q_m 80	T 25 °C; pH 7	Song and Jhung, 2017
	Zeolitic imidazolate framework–8	1H–benzotriazole	q_m 298.5	T 30 °C	Jiang et al., 2013
	Zeolitic imidazolate framework–8	5-tolyltriazole	q_m 396.8	T 30 °C	Jiang et al., 2013
	Metal organic framework–porous carbon	Ibuprofen	q_m 320	T 25 °C; pH 5.0–5.5	Bhadra et al., 2017
	Metal organic framework–porous carbon	Diclofenac sodium	q_m 400	T 25 °C; pH 5.0–5.5	Bhadra et al., 2017
	Silver nanoparticle-modified MWCNT	Sulfamethoxazole	q_m 118.58	pH 4	Song et al., 2016
	Mesoporous SBA-15	Carbamazepine	q_m 0.16	T 25 °C; pH 3	Bui and Choi, 2009
	Mesoporous SBA-15	Diclofenac	q_m 0.07	T 25 °C; pH 3	Bui and Choi, 2009
	Mesoporous SBA-15	Ibuprofen	q_m 0.34	T 25 °C; pH: 3	Bui and Choi, 2009
	Mesoporous SBA-15	Ketoprofen	q_m 0.41	T 25 °C; pH 3	Bui and Choi, 2009
	Mesoporous SBA-15	Clofibric	q_m 0.28	T 25 °C; pH 3	Bui and Choi, 2009
	Polyvinyl pyrrolidone -Fe_3O_4	Triclosan	q_m 52.63	pH 7	Alizadeh Fard et al., 2017
	Polyvinyl pyrrolidone -Fe_3O_4	Ketoprofen	q_m 83.33	pH 7	Alizadeh Fard et al., 2017
	Polyvinyl pyrrolidone -Fe_3O_4	Bisphenol-A	q_m 90.91	pH 7	Alizadeh Fard et al., 2017
	Polyvinyl pyrrolidone -Fe_3O_4	Estriol	q_m 56.17	pH 7	Alizadeh Fard et al., 2017
	Carboxymethyl cellulose-Fe/Mn	Ciprofloxacin	q_m 1172.25	pH 5	Yan et al., 2017

the resulting electrostatic interactions between them may influence the removal of triclosan and IBP by CNTs in water (Wang et al., 2015). Due to the presence of oxygenated functional groups on PPCPs and CNTs, the solution pH affects the protonation/deprotonation of these functional groups and alters the electrostatic interactions (Cho et al., 2011). The electrostatic interaction might contribute greatly to the adsorption

affinity of norfloxacin on the surface of MWCNTs (Yang et al., 2012). The higher adsorption capacity of oxytetracycline and diethyl phthalate on 3D GTs than pure GO and CNT-based adsorbents can be attributed to the synergistic effects of GO and CNTs in the micro-environment, the surface nano-substrate, and multiple active sites with the cooperative electrostatic and π-π interactions (Shen et al., 2017).

2.1.2.3. Hydrophobic interaction. Hydrophobic interaction is another mechanism for carbon materials to adsorb hydrophobic organic compounds (Nam et al., 2014; Pyrzynska et al., 2007). When the net charge density on the carbon material is zero and the emerging contaminants are in their molecular state, the hydrophobic interaction between them is at the strongest, and the adsorption capacity the largest (Lu et al., 2006; Piao et al., 2008). Besides, the adsorption is also affected by oxygen-containing functional groups on the adsorbents (Cho et al., 2008; Liao et al., 2008). Hydrophobic interaction is the main mechanism responsible for the pH-dependent adsorption of sulfonamides (Yu et al., 2015). Non-electrostatic hydrophobic interaction was also found between tetracycline and MWCNTs (Zhang et al., 2011).

2.1.2.4. Hydrogen bonding. Hydrogen bonds can also be formed between the benzene ring on the surface of CNTs as the electron donor and organic compounds containing oxygen-containing functional groups (Pan and Xing, 2008). The hydrogen bonding contributed greatly to the adsorption of 17β-estradiol (E2) and 17α-ethinylestradiol (EE2) on GO due to the high content of –OH groups on the GO surface (Sun et al., 2017).

2.1.3. Influencing factors

2.1.3.1. pH. The solution pH strongly controls the adsorption process of organic molecules, since it affects not only the surface charge of adsorbents, but also the protonation/deprotonation of pollutants according to their pKa. First, increasing pH might promote the dissociation of the hydrophobic adsorbate into hydrophilic and negatively charged species, thus affecting the hydrophobic and electrostatic interactions between the adsorbent and adsorbate. Second, a higher pH could increase the π donating ability of the adsorbate, thus enhancing the π-π electron donor-acceptor interaction (Liu et al., 2014). Depending on the pH, PPCPs will be protonated or deprotonated, resulting in their electrostatic interaction with the CNTs (Nam et al., 2014). The adsorption of sulfonamide to MWCNTs decreases as the pH increases, because the electron accepting abilities of the cationic amine group and the enol-enone groups on sulfonamide are weakened when these moieties are protonated at high pH (Ji et al., 2009). For the adsorption of triclosan to SWCNTs, better removal was observed at pH 4 and 7 than at 10 (Castro et al., 2017; Wang et al., 2015). The pH value (within 1–11) also significantly affects the adsorption of sulfadimethoxine, sulfamethoxazole, and sulfathiazole by MWCNTs, due to the changed sulfonamide species (Yu et al., 2015). The adsorption of ACT onto GO is almost independent of solution pH between 2 and 8, because at these pH values ACT remains mostly neutral and nonionic, and thus is unfavorable for electrostatic and π–π interactions with functional groups on the surface of GO (Moussavi et al., 2016). The adsorption of metformin on GO increased when the pH changed from 4.0 to 6.0, and then decreased from 6.0 to 11.0, which might be attributed to the changing surface charge on GO and the speciation of metformin (S. Zhu et al., 2017).

2.1.3.2. Ionic strength. An increase in ionic strength would be favorable to the adsorption processes, when there is electrostatic repulsion between the adsorbent and adsorbate. Also, a high ionic strength can have a strong "salting-out" effect on hydrophobic compounds, increasing the tendency of organic molecules to precipitate from the aqueous solution and adsorb to the nanoadsorbent (Grover and Ryall, 2005). When the ionic strength is increased from 10^{-3} to 10^{-2} M, for example, the adsorption of triclosan onto MWCNTs at pH 3 and 11 increased from 136.1 to 153.1 mg/g and from 80.8 to 105.8 mg/g, respectively (Zhou et al., 2013). The solubility of norfloxacin in water is decreased when NaCl or $CaCl_2$ is added, especially for $CaCl_2$ (Yang et al., 2012). The adsorption capacities of tetracycline on GO decreased upon increasing the Na^+ concentration (Gao et al., 2012). Moreover, the adsorption of thiamphenicol and IBP was decreased at increased ionic strength, and the same trend was observed to a lesser extent for diclofenac (DCF) and carbamazepine (Zhao et al., 2016). The addition of 0.5 g/L NaCl considerably inhibited the adsorption of ACT (by about 30%), which might be due to the aggregation of GO at high ionic strengths (Moussavi et al., 2016). The adsorption capacity of metformin on GO was reduced by increasing the NaCl concentration from 0 to 0.1 M, and this could be explained by the lower active coefficients of metformin, the competitive adsorption of Na^+, and the increasing aggregation of GO particles (S. Zhu et al., 2017).

2.1.3.3. Dissolved organic matters. The adsorption of sulfamethoxazole, thiamphenicol, and IBP was decreased with the increase of organic matter in the solution (Zhao et al., 2016). When the amount of dissolved humic acid was increased (up to 40 mg/L), the adsorption coefficients of the two sulfonamides decreased by 0.5–0.8 mg/kg, mainly due to direct competition for the adsorbent surface (Ji et al., 2009).

2.2. MOF nanomaterials

2.2.1. Adsorption capacity

The adsorption capacities of reported nanomaterials are summarized in Table 1. Zeolitic imidazole frameworks (ZIF)-magnetic GO shows a high adsorption capacity for benzotriazole (>300 mg/g) (Andrew Lin and Der Lee, 2016). The adsorption of the antibiotic nitroimidazole depended strongly on the type of functional groups on the MOFs (Seo et al., 2017). The adsorption of ZIF-8 for 1H–benzotriazole and 5-tolyltriazole follows pseudo-second-order kinetics, and fits the Langmuir adsorption model with the respective adsorption capacity of 298.5 and 396.8 mg/g (Jiang et al., 2013). Polyvinylpyrrolidone-coated iron oxide nanoparticles also showed efficient removal of bisphenol A and ketoprofen (98% and 95% removal, respectively, Alizadeh Fard et al., 2017). Carboxymethyl cellulose-Fe/Mn nanoadsorbent showed the maximum adsorption of 1172.25 mg/g for ciprofloxacin at pH 5 in water (Yan et al., 2017).

2.2.2. Adsorption mechanism

MOFs can adsorb pollutants in water via the following mechanisms: electrostatic interactions, Lewis acid–base interactions, H-bonding, and π–π interactions (Andrew Lin and Der Lee, 2016). The adsorption of nitroimidazole antibiotics on MOFs was attributed to H-bonding between the $-NO_2$ of nitroimidazole and $-NH_2$ of the modified MOFs (Seo et al., 2017). For the adsorption of IBP and DCF onto porous carbon derived from MOFs, the most probable reason for the relatively higher reduction in IBP is that there are many more H-bond acceptors in IBP than in DCF (Bhadra et al., 2017).

2.2.3. Influencing factors

2.2.3.1. pH. The pH could affect sulfamethoxazole sorption on MOFs: the Kd values slightly increased with pH from 2 to 4, then decreased at pH = 5–10 (Song et al., 2016). The adsorption capacities of ZIF-8 for 1H–benzotriazole and 5-tolyltriazole slightly decreased as the pH increased. ZIF-8 also exhibited appreciable amount of benzotriazole adsorption (~150 mg/g) at pH 8 and 9 (Jiang et al., 2013). The ZIFs–negatively-charged magnetic reduced GO exhibited relatively stable adsorption capacities for benzotriazole (BTA) at pH 4–9. Once the pH was raised to 10 (which is higher than the pKa value of 2), the decrease in adsorption became significant due to the inhibition of electrostatic adsorption by the negatively-charged species of BTA and GO (Andrew Lin and Der Lee, 2016). A urea- or melamine-modified MOF, MIL-101, displays stable

adsorption for saccharin (SAC) at pH 3–7, which could be attributed to the electrostatic attraction of negatively charged deprotonated form of SAC with positively charged MIL-101, and the stable H-bonding between the SAC anion and $-NH_2$ group on urea-MIL-101 (Seo et al., 2016). For the carboxymethyl cellulose binary oxide Fe-Mn nanoparticles (CMC-FMBO), at pH < 6.0, the sorption capacity of CIP increased with increasing pH due to the electrostatic attraction between the cationic form of CIP and increasingly negatively charged CMC-FMBO. At pH > 6.0, the sorption capacity declined, and this might be due to (1) the formation of anionic CIP that exhibited electrostatic repulsion with negatively charged CMC-FMBO, (2) increasing competitive adsorption of hydroxyl ions against anionic CIP, and (3) much less hydrophobic for the anionic form than the zwitterionic one (Yan et al., 2017). On a carbon-modified ZIF-8, the adsorption of IBP decreased with increasing pH, which showed that the electrostatic interaction was not the main process for IBP adsorption here (Bhadra et al., 2017). Two composites, MIL-101/sodium alginate (MIL-101/SA) and MIL-101/chitosan (MIL-101/CS), exhibited similar patterns of pH-dependent adsorption of three PPCPs (benzoic acid (BEN), IBP, and ketoprofen (KET)) with a maximum adsorption at pH ~4.0, suggesting again the predominant influence of pKa-dependent electrostatic attraction in adsorption (Zhuo et al., 2017). The decrease of adsorption over urea-modified MIL-101 with increasing pH can be explained by the electrostatic interaction between the negatively charged O in the $-NO_2$ group of the nitroimidazole antibiotics and the positive surface charge on MIL-101 (Seo et al., 2017).

2.2.3.2. Ionic strength. No significant change of the adsorption capacity of benzotriazole on ZIF was found in the presence of NaCl, $CaCl_2$, and $MgSO_4$ (Jiang et al., 2013). The removal of CIP by CMC-FMBO was enhanced in the presence of NaCl, possibly due to the decreased CIP solubility (i.e. salting out), and the promoted formation of adsorbent aggregates (i.e. squeezing out) (Yan et al., 2017). The salts have insignificant effects on the BTA adsorption to ZIF–GO (Andrew Lin and Der Lee, 2016). The adsorption of three PPCPs onto MIL-101/SA and MIL-101/CS decreased with increasing ionic concentration due to competition from Cl^-, while the adsorption was almost unchanged with the ionic concentration of >0.25 wt% (Zhuo et al., 2017).

2.2.3.3. Dissolved organic matter. The polyvinylpyrrolidone (PVP)-coated magnetite nanoparticles (NPs) showed good adsorption performance for bisphenol A and ketoprofen with 98 and 95% removal. PVP-coated NPs showed still good performance for the adsorption of these pollutants, while their removal by granular activated carbon (GAC) was significantly inhibited by the competitive inhibition of dissolved organic matter with micropollutants (Alizadeh Fard et al., 2017).

3. Photocatalysis

Photocatalytic oxidation is an advanced oxidation process for removing trace contaminants, which can be a polishing step to treat emerging and recalcitrant organic compounds. The main photocatalysts contain either single metal oxides (TiO_2, ZnO, and WO_3) or GO or CNT combined with catalytic components (e.g. TiO_2, $ZnFe_2O_4$, WO_3, C_3N_4, Nb_2O_5, Co_3O_4, and Cu_2O).

3.1. Photocatalytic property

Table 2 summarizes the photocatalysts and their degradation capacities. With TiO_2 catalyst, the removal efficiencies of DCF and naproxen (NPX) were 75% under Xe lamps after 2 h (Méndez-Arriaga et al., 2008). With TiO_2 concentrations of 10 and 20 mg/L, ~85% and 100% of IBP was degraded after 3 h, respectively (Choina et al., 2013). Using 5 mg/L TiO_2, hydroxybiphenyl, DCF, IBP, progesterone, triclosan, ofloxacin, acetaminophen, and caffeine were all completely degraded in <1 h (Miranda-García et al., 2011). A 72% degradation rate of atenolol can be achieved in 1 h with 1.5 g/L TiO_2 under solar irradiation (Bhatia et al., 2017). The degradation of triclosan by TiO_2 was very efficient and complete after about 1 h (Rafqah et al., 2006). Triclosan in water could also be degraded by 90% using ZnO under solar radiation in 90 min (Kosera et al., 2017). When using ZnO coated activated carbon fiber, 99% of tetracycline at 40 mg/L was degraded within 1 h under UV light (Tran and Lee, 2017). A 98% removal rate of sulfamethoxazole was achieved within 3 h under visible light irradiation using GO-WO_3 (W. Zhu et al., 2017). g-C_3N_4/Nb_2O_5 nano-heterostructures exhibited a high activity (81% removal) in the photooxidation of the drug amiloride (AML) (da Silva et al., 2017). The Gold@Silver@Silver chloride (Au@Ag@AgCl) core–double shells NPs were produced using *Momordica charantia* leaf extract, and the prepared material showed a degradation rate of 97% for IBP and 98% for clofibric acid (CA) at 10 mg/L in aqueous solution under solar irradiation (Devi and Ahmaruzzaman, 2017). The addition of g-C_3N_4 in TiO_2 resulted in a 2.3-times faster photodegradation rate for CA than for pristine TiO_2 under simulated solar irradiation (Chen et al., 2017).

3.2. Photocatalytic mechanisms

Among the many photocatalysts, TiO_2 is mostly preferred due to its chemical stability, acceptable band gap, ability to adsorb electrons, low cost, etc. (Gao and Wen, 2016). When the photon energy is equal to or greater than the energy gap ($h\nu \geq E_g$), photon impingement on the surface of nanosized TiO_2 forms a n/p controlled photocatalytic oxidation switch (Henderson, 2011). After the TiO_2 is excited, electron-hole pairs (e^-/h^+) are formed on the surface of the nanomaterial. The holes interact with H_2O on the surface to form highly oxidizing hydroxyl radicals (·OH) (Grabowska et al., 2012). The electrons, on the other hand, interact with the oxygen adsorbed on the TiO_2 surface to generate strongly oxidizing negative oxygen ion radicals ($O_2\cdot^-$). These strongly oxidative free radicals then oxidize and eventually degrade the emerging contaminants (Schneider et al., 2014). Various semiconductors and carbon-based carriers could significantly improve the photocatalytic degradation, via the high surface area, increased visible light absorption, the formation of an effective p–n type semiconductor nano-junction, and the suppression of the interfacial charge (e^- and h^+) recombination. For the composites of GO-TiO_2, GO-WO_3, and Co_3O_4–C_3N_4, the ·OH attack on the benzene ring or isoxazole ring was the main route of photodegradation of the antibiotics. For decatungstate anion immobilized on modified silica particles, the high degradation rates of LEV, atenolol (ATN), and trimethoprim (TMP) were all mediated by ·OH radicals, as confirmed using electron paramagnetic resonance spin trapping technique (Molinari et al., 2017).

Besides the indirect oxidizing radicals, the direct hole oxidation and electron reduction were important photocatalysis mechanisms. For a $ZnFe_2O_4$–Ag/rGO composite, direct oxidation by holes was important in the photodegradation besides the oxidation by the generated OH·, $O2\cdot^-$, and H_2O_2 under light condition (Khadgi et al., 2017). SiC/graphene catalyst could degrade PFOA by the photoinduced hydrodefluorination process via the Si — H/C — F redistribution under UV light excitation (Huang et al., 2016). Besides the radicals, Cl^0 also contributed the degradation of IBP and CA by the Gold@Silver@Silver chloride core–double shells NPs under solar irradiation (Devi and Ahmaruzzaman, 2017). The main degradation pathways of CA on g-C_3N_4/TiO_2 photocatalyst are e^- reduction, HO· oxidation, and $^1O_2$ attack reactions, according to mass spectrometry analysis and theoretical calculations (Chen et al., 2017).

3.3. Influencing factors

Numerous studies focused on the degradation of emerging contaminants via photocatalysis, and identified operational parameters that can affect the efficiency of these processes, such as the light intensity and wavelength, solution pH, and the presence of oxygen.

Table 2
Photodegradation of the emerging comtaminants in water.

Nanomaterial	Pollutant	Removal (%)	Treatment condition	Reference
TiO_2	Diclofenac	75	Xe lamp (1000 W, 290–400 nm); Time 2 h	Méndez-Arriaga et al., 2008
	Naproxen	75	Xe lamp (1000 W, 290–400 nm);Time 2 h	Méndez-Arriaga et al., 2008
	Hydroxybiphenyl	100	Solar UV lamp (30 W, <400 nm); Time 0.5 h	Miranda-García et al., 2011
	Diclofenac	100	Solar UV lamp (30 W, <400 nm); Time 0.5 h	Miranda-García et al., 2011
	Ibuprofen	100	Solar UV lamp (30 W, <400 nm); Time 0.5 h	Miranda-García et al., 2011
	Progesterone	100	Solar UV lamp (30 W, <400 nm); Time 0.5 h	Miranda-García et al., 2011
	Caffeine	100	Solar UV lamp (30 W, <400 nm); Time 0.5 h	Miranda-García et al., 2011
	Acetaminophen	100	Solar UV lamp (30 W, <400 nm); Time 0.5 h	Miranda-García et al., 2011
	Triclosan	100	Solar UV lamp (30 W, <400 nm); Time 0.5 h	Miranda-García et al., 2011
	Ofloxacin	100	Solar UV lamp (30 W, <400 nm); Time 0.5 h	Miranda-García et al., 2011
	Triclosan	100	Fluorescent lamp (15 W, 300–450 nm); Time 1 h	Rafqah et al., 2006
	Tetracycline	50	UV lamp (125 W, >254 nm), Time 1/6 h	Reyes et al., 2006
	Tetracycline	50	Solarium lamp (6 W, 300–400 nm); Time 1/3 h	Reyes et al., 2006
	Tetracycline	50	Black light lamp (160 W, 365 nm); Time 2 h	Reyes et al., 2006
	Benzophenone-3	93.7	Xe lamp (350 W); Time 0.5 h	Zúñiga-Benítez et al., 2016
	Sulfamethoxazole	100	UV-A light (450 W, 324–400 nm); Time 1 h	Hu et al., 2007
	Sulfamethazine	35	Osram Dulux lamp (9 W, 350/400 nm); Time 1 h	Kaniou et al., 2005
	Caffeine	51	Four UV- lamps (15 W, 273 nm); Time 4 h	Arfanis et al., 2017
	Salicylic acid	55	Four UV- lamps (15 W, 296 nm); Time 4 h	Arfanis et al., 2017
	Caffeine	92	Solar UV lamp (30 W, 273 nm); Time 2 h	Gil et al., 2017
	Diclofenac	47	Solar UV lamp (30 W, 450 nm); Time 2 h	Gil et al., 2017
	Ibuprofen	47	Solar UV lamp(30 W, 222 nm); Time 2 h	Gil et al., 2017
	Salicylic acid	22	Solar UV lamp(30 W, 296 nm); Time 2 h	Gil et al., 2017
Ni-TiO_2	Bisphenol A	100	Phillips lamp(25 W, 400–700 nm); Time 3.5 h	Blanco-Vega et al., 2017
Ag, Pd, or Pt-TiO_2	Perfluorooctanoic acid	100	Hg lamp (125 W, 365 nm); Time 5 h	Li et al., 2016
ZnO	Amoxicillin	100	UV lamp (6 W, 365 nm); Time 3 h	Elmolla and Chaudhuri, 2010
	Ampicillin	100	UV lamp (6 W, 365 nm); Time 3 h	Elmolla and Chaudhuri, 2010
	Cloxacillin	100	UV lamp (6 W, 365 nm); Time 3 h	Elmolla and Chaudhuri, 2010
	Sulfamethazine	92	Osram Dulux lamp (9 W, 350/400 nm); Time 1 h	Kaniou et al., 2005
	Ibuprofen	88	Hg lamp (125 W, 254 nm); Time 1.3 h	Rastkari et al., 2017
	Triclosan	100	Hg lamp (125 W, 200–300 nm)	Kosera et al., 2017
Ce-ZnO	Acelsulfame K	65	Xe arc lamp (1500 W, 290 nm); Time 1.5 h	Calza et al., 2017
WO_3	Atenolol	70	Luxtel Xenon lamp (175 W, >360 nm); Time 5 h	Longobucco et al., 2017
	Carbamazepine	60	Luxtel Xenon lamp (175 W, >360 nm); Time 5 h	Longobucco et al., 2017
	Acetaminophen	100	Xe lamp (1500 W, 300 nm); Time 2 h	Rey et al., 2015
	Metoprolol	100	Xe lamp (1500 W, 300 nm); Time 2 h	Rey et al., 2015
	Caffeine	100	Xe lamp (1500 W, 300 nm); Time 2 h	Rey et al., 2015
	Hydrochlorothiazide	100	Xe lamp (1500 W, 300 nm); Time 2 h	Rey et al., 2015
	Antipyrine	100	Xe lamp (1500 W, 300 nm); Time 2 h	Rey et al., 2015
	Sulfamethoxazole	100	Xe lamp (1500 W, 300 nm); Time 2 h	Rey et al., 2015
	Carbamazepine	100	Xe lamp (1500 W, 300 nm); Time 2 h	Rey et al., 2015
	Ketorolac	100	Xe lamp (1500 W, 300 nm); Time 2 h	Rey et al., 2015
	Diclofenac	100	Xe lamp (1500 W, 300 nm); Time 2 h	Rey et al., 2015
	Ibuprofen	100	Xe lamp (1500 W, 300 nm); Time 2 h	Rey et al., 2015
$Na_4W_{10}O_{32}$	Atenolol	100	Hg lamp (125 W, λ > 300 nm); Time 3 h	Molinari et al., 2017
	Levofloxacin	100		
	Trimethoprim	100		
Graphene oxide-TiO_2	Atenolol	72	Solar irradiation (1000 W); Time 1 h	Bhatia et al., 2017
	Caffeine	99	Solar UV lamp (30 W, <400 nm); Time 1 h	Linley et al., 2014
	Carbamzepine	99		
Graphene oxide-WO_3	Sulfamethoxazole	100	Xe arc lamp (200 W, 420–630 nm); Time 3 h	S. Zhu et al., 2017
Graphene oxide-Ag-$ZnFe_2O_4$	17α-ethinyl estradiol	100	Xe arc lamp (300 W, <400 nm); Time 1.5 h	Khadgi et al., 2017
Graphene oxide-Cu_2O	Sulfamethoxazole	100	Xe arc lamp (300 W, 420 nm); Time 2 h	Liu et al., 2016
Graphene oxide-Ag-$ZnFe_2O_4$	17α-ethinyl estradiol	80	Xe arc lamp (300 W, <400 nm); Time 4 h	Li et al., 2016
WO_3-g-C_3N_4	Sulfamethoxazole	80	Xe arc lamp (300 W, 420–630 nm); Time 4 h	Sun et al., 2017
Nb_2O_5-g-C_3N_4	Amiloride	80	Fluorescent lamps (15 W, 440 nm); Time 3 h	da Silva et al., 2017
Co_3O_4-g-C_3N_4	Tetracycline	90	Solar UV lamp (30 W, 357 nm); Time 3.3 h	Suyana et al., 2017
Au@Ag@AgCl	Ibuprofen	98	Solarium lamp (6 W, 300–400 nm); Time 2 h	Devi and Ahmaruzzaman, 2017
Cu-MnO_2	Benzotriazole	89	Solarium lamp (6 W, 300–400 nm); Time 1 h	Zhang et al., 2016
g-C_3N_4-TiO_2	Clofibric acid	85	Xe-lamp (350 W, 290 nm); Time 50 min	Chen et al., 2017
ZnO-activated carbon	Tetracycline	99	UV lamps (20 W, 365 nm); Time 1 h	Tran and Lee, 2017
C_3N_4-ZIF 8	Tetracycline	96	Solarium lamp (6 W, 300–400 nm); Time 1 h	Panneri et al., 2017
g-C_3N_4	Atrazine	100	Xe-lamp (1000 W, >400 nm); Time 1 h	Zheng et al., 2016

3.3.1. Light source

The light source affects the reaction according to both the wavelength and light intensity. At low light intensity, the photocatalytic reaction rate is proportional to the intensity of light (Herrmann, 1995). High photocatalytic conversion efficiency of formaldehyde by TiO_2 was observed under UV (Yang et al., 2007). No sulfamethoxazole degradation was observed in TiO_2 suspensions irradiated with only visible light (>400 nm), and direct photolysis of sulfamethoxazole by UV is slow (Hu et al., 2007). To achieve 50% degradation of triclosan in water, approximately 10, 20, and 120 min of irradiation was necessary for UV, solarium, and black light lamps, respectively (Reyes et al., 2006).

3.3.2. pH

The pH value can strongly influence the degree of particle aggregation, the band edge position, and the surface charge of semiconductor catalyst particles in the reaction solution, as well as the adsorption of

Fig. 1. Nanoadsorbents, emerging contaminants, and research focus on nanoadsorption during 1998–2017. CNT: carbon nanotube; GO: graphene oxide; CMC: caboxy methyl cellulose; MIL: chromium (III) terephthalat; PVP: polyvinylpyrrolidone; ZIF: zeolitic imidazole framework; PFOA: perfluorooctanoic acid; PFOS: perfluorooctane sulphonate; PFC: perfluorinated compound; EDC: endocrine disrupting chemical; PPCP: pharmaceutical and personal care product.

organic pollutants on their surface. In photocatalytic reactions, the effect of pH is related to the surface charge of the catalyst and the ionic form of the substrate (Zúñiga-Benítez et al., 2016). When the pH is below the point of zero charge, the catalyst particles are protonated and positively charged, while at higher pH the surface is deprotonated and more negatively charged (Choina et al., 2013). After 6 h of reaction, the photocatalytic degradation of amoxicillin, ampicillin, and ciclopirox by TiO_2 in water all reached the highest rate at pH 11 and the lowest rate at pH 5, since the pH changes both the morphology of the antibiotic and the catalyst (Elmolla and Chaudhuri, 2010). A slight rate increase was observed under alkaline pH, possibly due to changes in the acid-base speciation of sulfamethoxazole or the extent of its adsorption on TiO_2 (Hu et al., 2007).

3.3.3. Presence of oxidants

After adding an oxidant to the reaction system, it is captured on the surface of the catalyst, reducing the hole-electron recombination rate and promoting the formation of ·OH. The rate of benzophenone-3 degradation increases upon increasing the H_2O_2 concentration, but a decrease is observed when the concentration exceeds 128 mg/L (Zúñiga-Benítez et al., 2016). No sulfamethoxazole degradation occurs under strict anoxic conditions unless an external electron acceptor is provided; and the degradation rate is greater in O_2-sparged than air-sparged suspensions (Hu et al., 2007). In the photocatalytic oxidation of sulfamethoxazole, H_2O_2 can absorb light to promote the charge separation and therefore the oxidation reaction. The excessive H_2O_2 also acts as holes or hydroxyl trapping molecules, and reacts with TiO_2 to form a peroxide, which is detrimental to the photocatalytic degradation reaction (Kaniou et al., 2005).

3.4. Photocatalyst modification

In recent years, to improve the efficiency of photocatalysis, people have used a variety of means to modify the catalyst, mainly by metal or non-metallic element doping, precious metal deposition, and semiconductor recombination.

3.4.1. Doping

Non-metallic doping (N, C, S, Si, B, F) (Shi et al., 2011; Wang et al., 2009; Wang et al., 2012), metal doping (Fe, Nb, Sn, Co) (Le et al., 2012; Xu et al., 2012), and co-doping (S-N, N-F, Ni-Ni) (Breault and Bartlett, 2012; He et al., 2012) could all introduce impurity energy and enhance the visible light absorption of the catalyst.

Among non-metals, N-doping could reduce the band gap of TiO_2 and realize the photocatalytic response of visible light (Asahi, 2001). Si was implanted into the TiO_2 lattice to form Si—O—Ti bond, and the TiO_2 after doping can maintain the original morphology and have high thermal stability. As a result, a maximum UV light conversion of 31.8% was achieved, which is 1.9 times that of the undoped electrode, and the corresponding photoelectrocatalytic degradation efficiency for pentachlorophenol was 84.8% higher (Su et al., 2016). The carbon-doped g-C_3N_4 showed a reaction rate enhancement of 2.3–10.5 fold for the

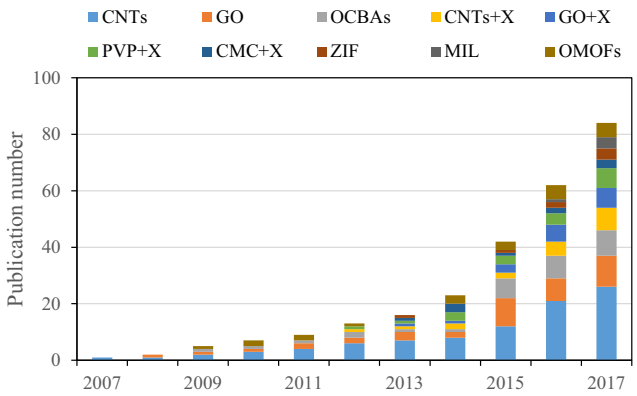

Fig. 2. Trend of studies on nanoadsorbents for removing emerging contaminants during 2007–2017. CNT: carbon nanotube; GO: graphene oxide; OCBA; other carbon-based adsorbent; CMC: caboxy methyl cellulose; MIL: chromium (III) terephthalat; PVP: polyvinylpyrrolidone; ZIF: zeolitic imidazole framework; OMOF; other metal-organic framework; X for CNT + X, GO + X, PVP + X, and CMC + X represents: Fe, Zn, Al, Si, N and so on.

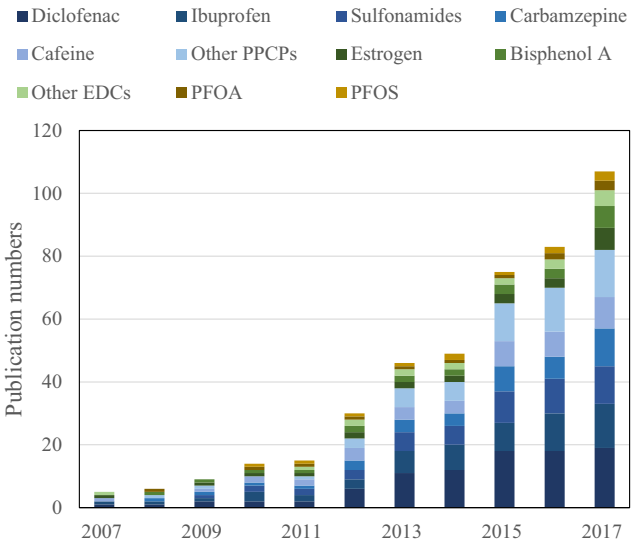

Fig. 3. Trend of studies on emerging contaminant removal using nanoadsorption during 2007–2017. PFOA: perfluorooctanoic acid; PFOA: perfluorooctane sulphonate; PFOS: perfluorinated compounds; EDC: endocrine disrupting chemical; PPCP: pharmaceutical and personal care product.

degradation of organic micropollutants compared to that of conventional, melamine-based g-C_3N_4 under simulated visible sunlight (Zheng et al., 2016). Following metal doping, the resultant photocatalytic properties are related to the electronic configuration of the dopant ions, and the metal ions affect the carrier recombination and electron transport (Nicole et al., 2001). Cerium-doped ZnO composites exhibit higher degradation of acesulfame K (ACE) than TiO_2, especially under visible light and in the presence of organic matter (Calza et al., 2017). Ag-, Pd-, and Pt-TiO_2 exhibited higher PFOA degradation of 57.7%, 94.2%, and 100%, respectively, compared with pure TiO_2 (31.1%), which was attributed to the storage of excess electrons in the conduction band by noble metal nanoparticles, when the holes in the valence band were used in PFOA degradation (Li et al., 2016).

3.4.2. Semiconductor compounds

The combination of TiO_2 and narrow bandgap semiconductors can reduce the energy required for light activation, thereby not only extending the spectral response of TiO_2 but also facilitating the separation of electron-hole pairs. The activity of Fe_2O_3/TiO_2 composite was found to be higher than that of pure Fe_2O_3 or TiO_2 under visible light, due to the presence of heterogeneous junctions between Fe_2O_3 and TiO_2 for the separation of carriers and the suppressed recombination of photogenerated electron-hole pairs (Yan et al., 2012). Cuprous oxide-reduced GO showed a 50% removal of sulfamethoxazole (SMX) within 120 min and 100% removal of methylene blue (MB) within 40 min under the visible light condition (Liu et al., 2016).

3.4.3. Precious metal deposition

The deposition of precious metals can improve the photocatalytic activity, because the metal and TiO_2 have different Fermi levels. When these two materials are in contact with each other, the electrons transfer from the Fermi level of TiO_2 to the Fermi level of the metal, and this effectively acts as an electron barrier to prevent the recombination of electrons and holes.

4. Bibliometrics on emerging contaminants, nanoadsorbents, and research focus

Recently, bibliometrics has been used as an important method for analyzing and predicting research trends. The keywords capture the main points in a study. Thus, keyword analysis is among the most effective methods in bibliometrics. Using the co-word analysis method, we can identify hot spots in the research field.

4.1. Trends for adsorption

"Emerging AND (Contaminant* OR Pollutant* OR micropollutant*) AND *sorption" were used to search titles, abstracts, and keywords of documents published between 1998 and 2017 in the Science Citation Index (SCI). We obtained 1010 related documents, and their keywords were analyzed using the open-source visualization and exploration software Gephi (Version 0.8.2). Trends in the adsorption studies could be visualized using the resulting co-word network.

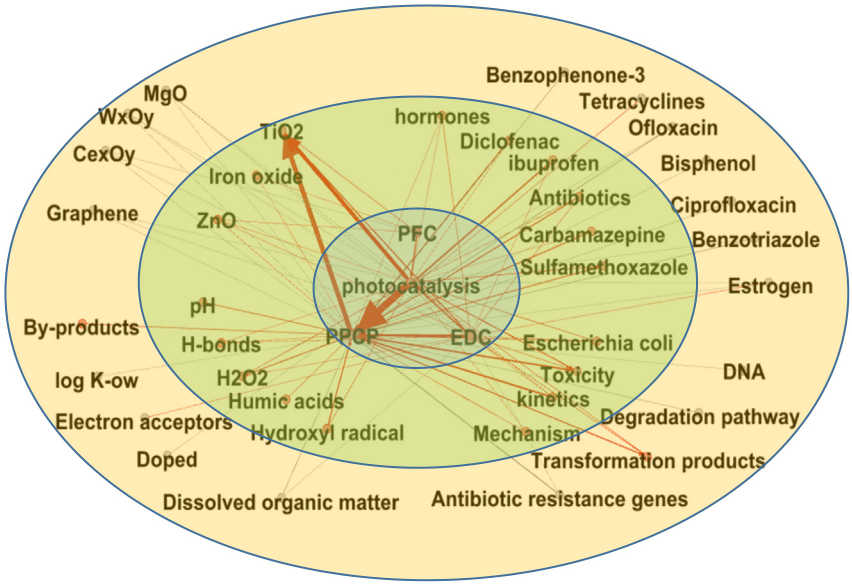

Fig. 4. Nanocatalyst, emerging contaminants, and research focus on nanophotocatalysis during 1998–2017.

The clustering of keywords was used to examine the main directions of related research on the global scale (Fig. 1). Over the past 20 years, the main adsorbents studied were carbon-based ones (CNTs, GO) and MOFs (CNTs + X, GO + X), polyvinylpyrrolidone (PVP) + X, carboxy methyl cellulose (CMC) + X, ZIF, and chromium (III) terephthalate (MIL). The main emerging contaminants studied were: antibiotics for PPCPs; bisphenol A, estrogen, and 17-beta-estradiol for EDCs; and perfluorooctanoic acid (PFOA) and perfluorooctane sulfonate (PFOS) for PFCs. The major research fields include adsorption kinetics, adsorption mechanism, isotherms, removal efficiency, toxicity, as well as the main influencing factors (e.g., competing adsorbates, dissolved organic matter, pH, temperature, and adsorption forces).

From 2011 to 2017, the number of papers on nanoadsorbents increased by 9.3 times (Fig. 2). Among the carbon-based ones, CNTs and GO were the most studied. The number of publications about these nanoadsorbents greatly increased after 2014, from 8 to 26 for CNTs in 2017. After 2011, the studies of MOF nanoadsorbents were greatly accelerated, and the ratio of relevant papers among those about nanoadsorbents increased from 22.2% to 45.2% in 2017. The studied frameworks mainly used CNTs, GO, and PVP for the organic component, and Fe, Zn, and Al for the metals. Besides, the ZIF (transition metal ions (Fe, Co, Cu, Zn) connected by imidazolate linkers) and MIL (trimers of Cr octahedra with terminal ligands linked by carboxylate ligands) are the newest nanoadsorbents, whose studies were significantly accelerated after 2016.

The literature on emerging pollutant removal using nanoadsorption continued to grow, with the highest number of 107 papers in 2017 (Fig. 3). Before 2009, half of the papers were about EDCs including bisphenol and estrogen. After 2009, there was an obviously increased interest in PPCPs, with the number of papers in 2017 being 8.2 times the number in 2009, and the ratio of PPCP studies in 2017 was 76.6% (Fig. 3). The main PPCPs examined include DCF, IBP, carbamazepine, caffeine, and NPX. Another interesting group was PFCs (PFOA and PFOS), with the number of papers gradually increased after 2009.

4.2. Trends for photocatalysis

"Emerging AND (contaminant* OR Pollutant* OR Micropollutant*) AND (Photocataly* OR Photodegrad*)" were used to search titles, abstracts, and keywords of the documents published between 1998 and 2017 in the SCI. We finally obtained 613 related documents, and their keywords were also analyzed by Gephi to obtain the co-word network and understand the research trends.

Based on keyword clustering analysis, Fig. 4 shows that the main photocatalysts considered by researchers are TiO_2, ZnO, MgO, WO_3, and GO. The main emerging contaminants are DCF, IBP, NPX, triclosan, and carbamazepine for PPCPs; and bisphenol and estrogen for EDCs. The main research fields were kinetics, photocatalytic mechanism, photolysis, degradation pathways, transformation product toxicity, as well as the influencing factors (including the dissolved organic matter, oxidation, pH, and modification on the photocatalyst).

In 2017, the number of papers on nanomaterials for photocatalysis increased by 6.2 times compared to that in 2011 (Fig. 5), and the most studied nanomaterials were TiO_2 and ZnO, either used singly or in combination. After 2014, the studies of WO_3, Bi_xO_y, and GO + X greatly increased by 4.1 times for the 3 categories in 2017.

Similar to the case of adsorption, the number of published studies on removing emerging pollutants by nanophotocatalysis increases year by year especially after 2012, with 87 papers in 2017. Before 2009, the studies of EDCs constituted half for the emerging contaminants. After 2009, the research of PPCPs was obviously intensified, with the number of publications increased by 89.7% from 2009 to 2017 (Fig. 6).

5. Conclusions and recommendations

We provided a systematic review and bibliometric analysis on nanomaterials for removing emerging pollutants in water by adsorption and/or photocatalysis processes. While a majority of studies up to 2009 were devoted to EDCs, there was clearly increased interest in PPCPs afterwards. Both the adsorption and photocatalysis approaches showed great potential for removing emerging pollutants from water. For the adsorption approach, CNT- and GO-based adsorbents have attracted the most interest, with the main adsorption mechanisms being hydrophobic effect, π-π interactions, hydrogen bonding, covalent bonding, and electrostatic interactions. Recently, the MOF nanomaterials showed great capacities for removing these pollutants via adsorption. TiO_2 and ZnO were the main nanomaterials studied for photocatalysis, while after 2014 the TiO_2- and GO-based frameworks have been greatly developed. The significant factors affecting photocatalysis are the light conditions, presence of oxidants, pH, and surface modification.

The following points are worthy of special attention in future relevant studies. (1) Combined MOF nanomaterials should be developed to enhance the adsorption as well as the synergistic photocatalysis. (2) New modification methods for the photocatalysts can improve the degradation efficiencies and widen the usable light wavelength. (3) The relationship between molecular structure and adsorption- and photocatalysis-based technologies should be clarified. (4) The efficiencies of the new technologies should be tested for real wastewater at large scales, and in the presence of dissolved organic matter and other coexisting substances.

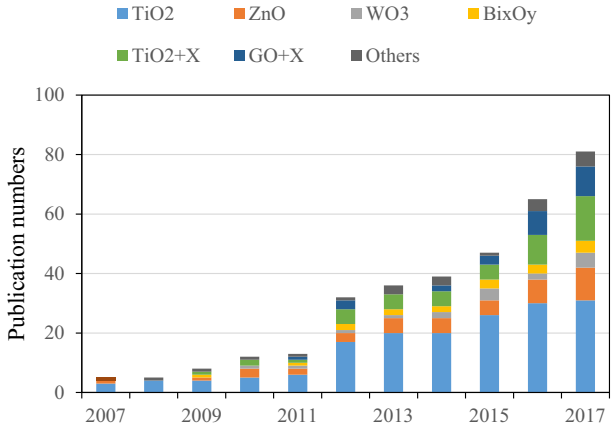

Fig. 5. Trend of studies on nanocatalyst for the photodegrading emerging contaminants during 2007–2017. X for TiO_2 + X and GO + X reprents Fe_3O_4, WO_3, ZnO, $BiVO_4$ and In_2O_3.

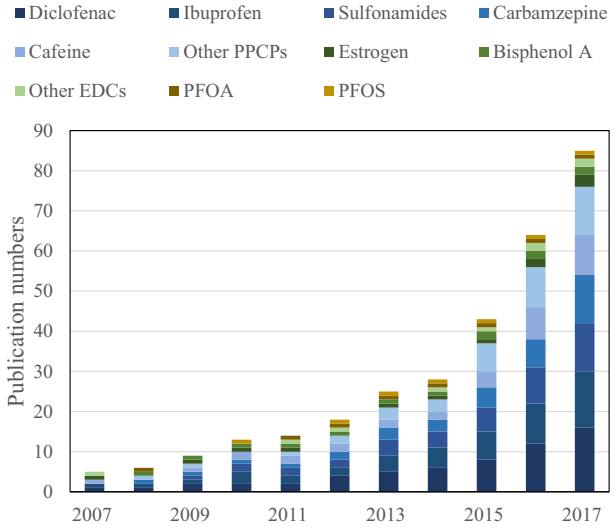

Fig. 6. Trend of studies on emerging contaminant removal using photocatalysis during 2007–2017.

Acknowledgement

This study was financially supported by National Natural Science Foundation of China (No. 314 21407112) and Natural Science Foundation of Tianjin (No. 17JCQNJC08800).

The authors declare no financial/commercial conflicts of interest.

References

Alder, A.C., Schaffner, C., Majewsky, M., Klasmeier, J., Fenner, K., 2010. Fate of β-blocker human pharmaceuticals in surface water: comparison of measured and simulated concentrations in the Glatt Valley Watershed, Switzerland. Water Res. 44, 936–948.

Alizadeh Fard, M., Vosoogh, A., Barkdoll, B., Aminzadeh, B., 2017. Using polymer coated nanoparticles for adsorption of micropollutants from water. Colloids Surf. A Physicochem. Eng. Asp. 531, 189–197.

Andrew Lin, K.Y., Der Lee, W., 2016. Self-assembled magnetic graphene supported ZIF-67 as a recoverable and efficient adsorbent for benzotriazole. Chem. Eng. J. 284, 1017–1027.

Apul, O.G., Karanfil, T., 2015. Adsorption of synthetic organic contaminants by carbon nanotubes: a critical review. Water Res. 68, 34–55.

Arfanis, M.K., Adamou, P., Moustakas, N.G., Triantis, T.M., Kontos, A.G., Falaras, P., 2017. Photocatalytic degradation of salicylic acid and caffeine emerging contaminants using titania nanotubes. Chem. Eng. J. 310, 525–536.

Asahi, R., 2001. Visible-light Photocatalysis in nitrogen-doped titanium oxides. Science 293, 269–271.

Behera, S.K., Kim, H.W., Oh, J.E., Park, H.S., 2011. Occurrence and removal of antibiotics, hormones and several other pharmaceuticals in wastewater treatment plants of the largest industrial city of Korea. Sci. Total Environ. 409, 4351–4360.

Benotti, M.J., Trenholm, R.A., Vanderford, B.J., Holady, J.C., Stanford, B.D., Snyder, S.A., 2009. Pharmaceuticals and endocrine disrupting compounds in U.S. drinking water. Environ. Sci. Technol. 43, 597–603.

Bhadra, B.N., Ahmed, I., Kim, S., Jhung, S.H., 2017. Adsorptive removal of ibuprofen and diclofenac from water using metal-organic framework-derived porous carbon. Chem. Eng. J. 314, 50–58.

Bhatia, V., Malekshoar, G., Dhir, A., Ray, A.K., 2017. Enhanced photocatalytic degradation of atenolol using graphene TiO_2 composite. J. Photochem. Photobiol. A Chem. 332, 182–187.

Blanco-Vega, M.P., Guzmán-Mar, J.L., Villanueva-Rodríguez, M., Maya-Treviño, L., Garza-Tovar, L.L., Hernández-Ramírez, A., Hinojosa-Reyes, L., 2017. Photocatalytic elimination of bisphenol A under visible light using Ni-doped TiO_2 synthesized by microwave assisted sol-gel method. Mater. Sci. Semicond. Process. 71, 275–282.

Breault, T.M., Bartlett, B.M., 2012. Lowering the band gap of anatase-structured TiO_2 by coalloying with Nb and N: electronic structure and photocatalytic degradation of methylene blue dye. J. Phys. Chem. C 116, 5986–5994.

Bui, T.X., Choi, H., 2009. Adsorptive removal of selected pharmaceuticals by mesoporous silica SBA-15. J. Hazard. Mater. 168, 602–608.

Calza, P., Gionco, C., Giletta, M., Kalaboka, M., Sakkas, V.A., Albanis, T., Paganini, M.C., 2017. Assessment of the abatement of acelsulfame K using cerium doped ZnO as photocatalyst. J. Hazard. Mater. 323, 471–477.

Carabineiro, S.A.C., Thavorn-Amornsri, T., Pereira, M.F.R., Serp, P., Figueiredo, J.L., 2012. Comparison between activated carbon, carbon xerogel and carbon nanotubes for the adsorption of the antibiotic ciprofloxacin. Catal. Today 186, 29–34.

Castiglioni, S., Bagnati, R., Fanelli, R., Pomati, F., Calamari, D., Zuccato, E., 2006. Removal of pharmaceuticals in sewage treatment plants in Italy. Environ. Sci. Technol. 40, 357–363.

Castro, S.M., Araújo, A.B., Nogueira, R.F.P., Guerini, S., 2017. Adsorption of triclosan on single wall carbon nanotubes: a first principle approach. Appl. Surf. Sci. 403, 519–524.

Chen, W., Duan, L., Zhu, D., Chen, W.E.I., Duan, L.I.N., 2007. Adsorption of polar and nonpolar organic chemicals to carbon nanotubes adsorption of polar and nonpolar organic chemicals to carbon nanotubes. Environ. Sci. Technol. 41, 8295–8300.

Chen, J., Chen, W., Zhu, D., 2008. Adsorption of nonionic aromatic compounds to single-walled carbon nanotubes: effects of aqueous solution chemistry. Environ. Sci. Technol. 42, 7225–7230.

Chen, P., Wang, F., Zhang, Q., Su, Y., Shen, L., Yao, K., Chen, Z.F., Liu, Y., Cai, Z., Lv, W., Liu, G., 2017. Photocatalytic degradation of clofibric acid by g-C_3N_4/P25 composites under simulated sunlight irradiation: the significant effects of reactive species. Chemosphere 172, 193–200.

Cho, H.H., Smith, B.A., Wnuk, J.D., Fairbrother, D.H., Ball, W.P., 2008. Influence of surface oxides on the adsorption of naphthalene onto multiwalled carbon nanotubes. Environ. Sci. Technol. 42, 2899–2905.

Cho, H.H., Huang, H., Schwab, K., 2011. Effects of solution chemistry on the adsorption of ibuprofen and triclosan onto carbon nanotubes. Langmuir 27, 12960–12967.

Choina, J., Kosslick, H., Fischer, C., Flechsig, G.U., Frunza, L., Schulz, A., 2013. Photocatalytic decomposition of pharmaceutical ibuprofen pollutions in water over titania catalyst. Appl. Catal. B Environ. 129, 589–598.

Devi, T.B., Ahmaruzzaman, M., 2017. Bio-inspired facile and green fabrication of Au@Ag@AgCl core–double shells nanoparticles and their potential applications for elimination of toxic emerging pollutants: a green and efficient approach for wastewater treatment. Chem. Eng. J. 317, 726–741.

Dong, S., Sun, Y., Wu, J., Wu, B., Creamer, A.E., Gao, B., 2016. Graphene oxide as filter media to remove levofloxacin and lead from aqueous solution. Chemosphere 150, 759–764.

Elmolla, E.S., Chaudhuri, M., 2010. Photocatalytic degradation of amoxicillin, ampicillin and cloxacillin antibiotics in aqueous solution using UV/TiO2 and UV/H2O2/TiO2 photocatalysis. Desalination 252, 46–52.

Ersan, G., Apul, O.G., Perreault, F., Karanfil, T., 2017. Adsorption of organic contaminants by graphene nanosheets: a review. Water Res. 126, 385–398.

Gao, D.W., Wen, Z.D., 2016. Phthalate esters in the environment: a critical review of their occurrence, biodegradation, and removal during wastewater treatment processes. Sci. Total Environ. 541, 986–1001.

Gao, Y., Li, Y., Zhang, L., Huang, H., Hu, J., Shah, S.M., Su, X., 2012. Adsorption and removal of tetracycline antibiotics from aqueous solution by graphene oxide. J. Colloid Interface Sci. 368, 540–546.

Gil, A., García, A.M., Fernández, M., Vicente, M.A., González-Rodríguez, B., Rives, V., Korili, S.A., 2017. Effect of dopants on the structure of titanium oxide used as a photocatalyst for the removal of emergent contaminants. J. Ind. Eng. Chem. 53, 183–191.

Grabowska, E., Reszczyńska, J., Zaleska, A., 2012. Mechanism of phenol photodegradation in the presence of pure and modified-TiO_2: a review. Water Res. 46, 5453–5471.

Grover, P.K., Ryall, R.L., 2005. Critical appraisal of salting-out and its implications for chemical and biological sciences. Chem. Rev. 105, 1–10.

He, Z., Que, W., Chen, J., Yin, X., He, Y., Ren, J., 2012. Photocatalytic degradation of methyl orange over nitrogen-fluorine codoped TiO_2 nanobelts prepared by solvothermal synthesis. ACS Appl. Mater. Interfaces 4, 6816–6826.

Heberer, T., 2002. Occurrence, fate, and removal of pharmaceutical residues in the aquatic environment: a review of recent research data. Toxicol. Lett. 131, 5–17.

Henderson, M.A., 2011. A surface science perspective on TiO_2 photocatalysis. Surf. Sci. Rep. 66, 185–297.

Herrmann, J.M., 1995. Heterogeneous photocatalysis: an emerging discipline involving multiphase systems. Catal. Today 24, 157–164.

Hu, L., Flanders, P.M., Miller, P.L., Strathmann, T.J., 2007. Oxidation of sulfamethoxazole and related antimicrobial agents by TiO_2 photocatalysis. Water Res. 41, 2612–2626.

Huang, D., Yin, L., Niu, J., 2016. Photoinduced hydrodefluorination mechanisms of perfluorooctanoic acid by the SiC/graphene catalyst. Environ. Sci. Technol. 50, 5857–5863.

Jauris, I.M., Matos, C.F., Zarbin, A.J.G., Umpierres, C.S., Saucier, C., Lima, E.C., Fagan, S.B., Zanella, I., Machado, F.M., 2017. Adsorption of anti-inflammatory nimesulide by graphene materials: a combined theoretical and experimental study. Phys. Chem. Chem. Phys. 19, 22099–22110.

Ji, L., Chen, W., Zheng, S., Xu, Z., Zhu, D., 2009. Adsorption of sulfonamide antibiotics to multiwalled carbon nanotubes. Langmuir 25, 11608–11613.

Ji, L., Chen, W., Bi, J., Zheng, S., Xu, Z., Zhu, D., Alvarez, P.J., 2010a. Adsorption of tetracycline on single-walled and multi-walled carbon nanotubes as affected by aqueous solution chemistry. Environ. Toxicol. Chem. 29, 2713–2719.

Ji, L., Shao, Y., Xu, Z., Zheng, S., Zhu, D., 2010b. Adsorption of monoaromatic compounds and pharmaceutical antibiotics on carbon nanotubes activated by KOH etching. Environ. Sci. Technol. 44, 6429–6436.

Jiang, J.Q., Yang, C.X., Yan, X.P., 2013. Zeolitic imidazolate framework-8 for fast adsorption and removal of benzotriazoles from aqueous solution. ACS Appl. Mater. Interfaces 5, 9837–9842.

Kaniou, S., Pitarakis, K., Barlagianni, I., Poulios, I., 2005. Photocatalytic oxidation of sulfamethazine. Chemosphere 60, 372–380.

Khadgi, N., Upreti, A.R., Li, Y., 2017. Simultaneous bacterial inactivation and degradation of an emerging pollutant under visible light by $ZnFe_2O_4$ co-modified with Ag and rGO. RSC Adv. 7, 27007–27016.

Kim, H., Hwang, Y.S., Sharma, V.K., 2014. Adsorption of antibiotics and iopromide onto single-walled and multi-walled carbon nanotubes. Chem. Eng. J. 255, 23–27.

Kleywegt, S., Pileggi, V., Yang, P., Hao, C., Zhao, X., Rocks, C., Thach, S., Cheung, P., Whitehead, B., 2011. Pharmaceuticals, hormones and bisphenol A in untreated source and finished drinking water in Ontario, Canada - occurrence and treatment efficiency. Sci. Total Environ. 409, 1481–1488.

Kosera, V.S., Cruz, T.M., Chaves, E.S., Tiburtius, E.R.L., 2017. Triclosan degradation by heterogeneous photocatalysis using ZnO immobilized in biopolymer as catalyst. J. Photochem. Photobiol. A Chem. 344, 184–191.

Kumar, A., Kumar, A., Sharma, G., Naushad, M., Veses, R.C., Ghfar, A.A., Stadler, F.J., Khan, M.R., 2017. Solar-driven photodegradation of 17-β-estradiol and ciprofloxacin from waste water and CO_2 conversion using sustainable coal-char/polymeric-g-C_3N_4/RGO metal-free nano-hybrids. New J. Chem. 41, 10208–10224.

Kumar, K.A., Mohan, V.S., 2012. Removal of natural and synthetic endocrine disrupting estrogens by multi-walled carbon nanotubes (MWCNT) as adsorbent: Kinetic and mechanistic evaluation. Sep. Purif. Technol. 87, 22–30.

Le, T.T., Akhtar, M.S., Park, D.M., Lee, J.C., Yang, O.B., 2012. Water splitting on Rhodamine-B dye sensitized Co-doped TiO_2 catalyst under visible light. Appl. Catal. B Environ. 111–112, 397–401.

Li, M., Yu, Z., Liu, Q., Sun, L., Huang, W., 2016. Photocatalytic decomposition of perfluorooctanoic acid by noble metallic nanoparticles modified TiO_2. Chem. Eng. J. 286, 232–238.

Liao, Q., Sun, J., Gao, L., 2008. The adsorption of resorcinol from water using multi-walled carbon nanotubes. Colloids Surf. A Physicochem. Eng. Asp. 312, 160–165.

Linley, S., Liu, Y., Ptacek, C.J., Blowes, D.W., Gu, F.X., 2014. Recyclable graphene oxide-supported titanium dioxide photocatalysts with tunable properties. ACS Appl. Mater. Interfaces 6, 4658–4668.

Liu, H., Zhang, J., Bao, N., Cheng, C., Ren, L., Zhang, C., 2012. Textural properties and surface chemistry of lotus stalk-derived activated carbons prepared using different phosphorus oxyacids: adsorption of trimethoprim. J. Hazard. Mater. 235–236, 367–375.

Liu, F.F., Zhao, J., Wang, S., Du, P., Xing, B., 2014. Effects of solution chemistry on adsorption of selected pharmaceuticals and personal care products (PPCPs) by graphenes and carbon nanotubes. Environ. Sci. Technol. 48, 13197–13206.

Liu, S.H., Wei, Y.S., Lu, J.S., 2016. Visible-light-driven photodegradation of sulfamethoxazole and methylene blue by Cu_2O/rGO photocatalysts. Chemosphere 154, 118–123.

Longobucco, G., Pasti, L., Molinari, A., Marchetti, N., Caramori, S., Cristino, V., Boaretto, R., Bignozzi, C.A., 2017. Photoelectrochemical mineralization of emerging contaminants at porous WO_3 interfaces. Appl. Catal. B Environ. 204, 273–282.
Loos, R., Locoro, G., Comero, S., Contini, S., Schwesig, D., Werres, F., Balsaa, P., Gans, O., Weiss, S., Blaha, L., Bolchi, M., Gawlik, B.M., 2010. Pan-European survey on the occurrence of selected polar organic persistent pollutants in ground water. Water Res. 44, 4115–4126.
Lu, C., Chung, Y., Chang, K., 2006. Adsorption thermodynamic and kinetic studies of trihalomethanes on multiwalled carbon nanotubes. J. Hazard. Mater. 138, 304–310.
Maeng, S.K., Ameda, E., Sharma, S.K., Grützmacher, G., Amy, G.L., 2010. Organic micropollutant removal from wastewater effluent-impacted drinking water sources during bank filtration and artificial recharge. Water Res. 44, 4003–4014.
Méndez-Arriaga, F., Esplugas, S., Giménez, J., 2008. Photocatalytic degradation of non-steroidal anti-inflammatory drugs with TiO_2 and simulated solar irradiation. Water Res. 42, 585–594.
Miranda-García, N., Suárez, S., Sánchez, B., Coronado, J.M., Malato, S., Maldonado, M.I., 2011. Photocatalytic degradation of emerging contaminants in municipal wastewater treatment plant effluents using immobilized TiO_2 in a solar pilot plant. Appl. Catal. B Environ. 103, 294–301.
Molinari, A., Sarti, E., Marchetti, N., Pasti, L., 2017. Degradation of emerging concern contaminants in water by heterogeneous photocatalysis with $Na_4W_{10}O_{32}$. Appl. Catal. B Environ. 203, 9–17.
Moussavi, G., Hossaini, Z., Pourakbar, M., 2016. High-rate adsorption of acetaminophen from the contaminated water onto double-oxidized graphene oxide. Chem. Eng. J. 287, 665–673.
Nam, S.-W., Choi, D.-J., Kim, S.-K., Her, N., Zoh, K.-D., 2014. Adsorption characteristics of selected hydrophilic and hydrophobic micropollutants in water using activated carbon. J. Hazard. Mater. 270, 144–152.
Nicole, J., Tsiplakides, D., Pliangos, C., Verykios, X., Comninellis, C., Vayenas, C., 2001. Electrochemical promotion and metal–support interactions. J. Catal. 204, 23–34.
Pan, B., Xing, B., 2008. Adsorption mechanisms of organic chemicals on carbon nanotubes. Environ. Sci. Technol. 42, 9005–9013.
Panneri, S., Thomas, M., Ganguly, P., Nair, B.N., Mohamed, A.P., Warrier, K.G.K., Hareesh, U.S., 2017. C_3N_4 anchored ZIF 8 composites: photo-regenerable, high capacity sorbents as adsorptive photocatalysts for the effective removal of tetracycline from water. Catal. Sci. Technol. 7, 2118–2128.
Peng, X., Yu, Y., Tang, C., Tan, J., Huang, Q., Wang, Z., 2008. Occurrence of steroid estrogens, endocrine-disrupting phenols, and acid pharmaceutical residues in urban riverine water of the Pearl River Delta, South China. Sci. Total Environ. 397, 158–166.
Piao, L., Liu, Q., Li, Y., Wang, C., 2008. Adsorption of L-phenylalanine on single-walled carbon nanotubes. J. Phys. Chem. C 112, 2857–2863.
Pyrzynska, K., Stafiej, A., Biesaga, M., 2007. Sorption behavior of acidic herbicides on carbon nanotubes. Microchim. Acta 159, 293–298.
Qu, X., Alvarez, P.J.J., Li, Q., 2013. Applications of nanotechnology in water and wastewater treatment. Water Res. 47, 3931–3946.
Rafqah, S., Wong-Wah-Chung, P., Nelieu, S., Einhorn, J., Sarakha, M., 2006. Phototransformation of triclosan in the presence of TiO_2 in aqueous suspension: mechanistic approach. Appl. Catal. B Environ. 66, 119–125.
Rastkari, N., Eslami, A., Nasseri, S., Piroti, E., Asadi, A., 2017. Optimizing parameters on nanophotocatalytic degradation of ibuprofen using UVC/ZnO processes by response surface methodology. Pol. J. Environ. Stud. 26, 785–794.
Ratola, N., Cincinelli, A., Alves, A., Katsoyiannis, A., 2012. Occurrence of organic microcontaminants in the wastewater treatment process. A mini review. J. Hazard. Mater. 239–240, 1–18.
Rey, A., Mena, E., Chávez, A.M., Beltrán, F.J., Medina, F., 2015. Influence of structural properties on the activity of WO_3 catalysts for visible light photocatalytic ozonation. Chem. Eng. Sci. 126, 80–90.
Reyes, C., Fernández, J., Freer, J., Mondaca, M.A., Zaror, C., Malato, S., Mansilla, H.D., 2006. Degradation and inactivation of tetracycline by TiO_2 photocatalysis. J. Photochem. Photobiol. A Chem. 184, 141–146.
Richardson, S.D., Ternes, T.A., 2011. Water analysis: emerging contaminants and current issues. Anal. Chem. 83, 4614–4648.
Rivera-Utrilla, J., Sánchez-Polo, M., Ferro-García, M.Á., Prados-Joya, G., Ocampo-Pérez, R., 2013. Pharmaceuticals as emerging contaminants and their removal from water. A review. Chemosphere 93, 1268–1287.
Schneider, J., Matsuoka, M., Takeuchi, M., Zhang, J., Horiuchi, Y., Anpo, M., Bahnemann, D.W., 2014. Understanding TiO_2 photocatalysis: mechanisms and materials. Chem. Rev. 114, 9919–9986.
Seo, P.W., Khan, N.A., Hasan, Z., Jhung, S.H., 2016. Adsorptive removal of artificial sweeteners from water using metal-organic frameworks functionalized with urea or melamine. ACS Appl. Mater. Interfaces 8, 29799–29807.
Seo, P.W., Khan, N.A., Jhung, S.H., 2017. Removal of nitroimidazole antibiotics from water by adsorption over metal–organic frameworks modified with urea or melamine. Chem. Eng. J. 315, 92–100.
Shan, C., Tong, M., 2013. Efficient removal of trace arsenite through oxidation and adsorption by magnetic nanoparticles modified with Fe-Mn binary oxide. Water Res. 47, 3411–3421.
Shen, Y., Zhu, X., Zhu, L., Chen, B., 2017. Synergistic effects of 2D graphene oxide nanosheets and 1D carbon nanotubes in the constructed 3D carbon aerogel for high performance pollutant removal. Chem. Eng. J. 314, 336–346.
Shi, W., Chen, Q., Xu, Y., Wu, D., Huo, C.F., 2011. Investigation of the silicon concentration effect on Si-doped anatase TiO_2 by first-principles calculation. J. Solid State Chem. 184, 1983–1988.
da Silva, G.T.S.T., Carvalho, K.T.G., Lopes, O.F., Ribeiro, C., 2017. g-C_3N_4/Nb_2O_5heterostructures tailored by sonochemical synthesis: enhanced photocatalytic performance in oxidation of emerging pollutants driven by visible radiation. Appl. Catal. B Environ. 216, 70–79.
Song, J.Y., Jhung, S.H., 2017. Adsorption of pharmaceuticals and personal care products over metal-organic frameworks functionalized with hydroxyl groups: quantitative analyses of H-bonding in adsorption. Chem. Eng. J. 322, 366–374.
Song, Q., Wang, H., Yang, B., Wang, F., Sun, X., 2016. A novel adsorbent of Ag-FMWCNTs for the removal of SMX from aqueous solution. RSC Adv. 6, 75855–75861.
Stackelberg, P.E., Furlong, E.T., Meyer, M.T., Zaugg, S.D., Henderson, A.K., Reissman, D.B., 2004. Persistence of pharmaceutical compounds and other organic wastewater contaminants in a conventional drinking-water-treatment plant. Sci. Total Environ. 329, 99–113.
Su, H., Lin, Y., Wang, Z., Wong, Y.L.E., Chen, X., Chan, T.W.D., 2016. Magnetic metal–organic framework–titanium dioxide nanocomposite as adsorbent in the magnetic solid-phase extraction of fungicides from environmental water samples. J. Chromatogr. A 1466, 21–28.
Sun, W., Li, M., Zhang, W., Wei, J., Chen, B., Wang, C., 2017. Sediments inhibit adsorption of 17β-estradiol and 17α-ethinylestradiol to carbon nanotubes and graphene oxide. Environ. Sci. Nano. 4, 1900–1910.
Suyana, P., Ganguly, P., Nair, B.N., Mohamed, A.P., Warrier, K.G.K., Hareesh, U.S., 2017. Co_3O_4–C_3N_4 p–n nano-heterojunctions for the simultaneous degradation of a mixture of pollutants under solar irradiation. Environ. Sci. Nano 4, 212–221.
Tian, Y., Gao, B., Morales, V.L., Chen, H., Wang, Y., Li, H., 2013. Chemosphere removal of sulfamethoxazole and sulfapyridine by carbon nanotubes in fixed-bed columns. Chemosphere 90, 2597–2605.
Tran Thi, V.H., Lee, B.K., 2017. Great improvement on tetracycline removal using ZnO rod-activated carbon fiber composite prepared with a facile microwave method. J. Hazard. Mater. 324, 329–339.
Wang, J., Tafen, D.N., Lewis, J.P., Hong, Z., Manivannan, A., Zhi, M., Li, M., Wu, N., 2009. Origin of photocatalytic activity of nitrogen-doped TiO_2 Nanobelts. J. Am. Chem. Soc. 131, 12290–12297.
Wang, X., Blackford, M., Prince, K., Caruso, R.A., 2012. Preparation of boron-doped porous titania networks containing gold nanoparticles with enhanced visible-light photocatalytic activity. ACS Appl. Mater. Interfaces 4, 476–482.
Wang, Y., Zhu, J., Huang, H., Cho, H.-H., 2015. Carbon nanotube composite membranes for microfiltration of pharmaceuticals and personal care products: capabilities and potential mechanisms. J. Membr. Sci. 479, 165–174.
Xu, M., Da, P., Wu, H., Zhao, D., Zheng, G., 2012. Controlled Sn-doping in TiO_2 nanowire photoanodes with enhanced photoelectrochemical conversion. Nano Lett. 12, 1503–1508.
Yan, X., Zou, C., Gao, X., Gao, W., 2012. ZnO/TiO_2 core–brush nanostructure: processing, microstructure and enhanced photocatalytic activity. J. Mater. Chem. 22, 5629.
Yan, Z. li, Liu, Y. guo, Tan, X. fei, Liu, S. bo, Zeng, G. ming, Jiang, L. hua, Li, M. fang, Zhou, Z., Liu, S., Cai, X. xi, 2017. Immobilization of aqueous and sediment-sorbed ciprofloxacin by stabilized Fe-Mn binary oxide nanoparticles: influencing factors and reaction mechanisms. Chem. Eng. J. 314, 612–621.
Yang, L., Liu, Z., Shi, J., Zhang, Y., Hu, H., Shangguan, W., 2007. Degradation of indoor gaseous formaldehyde by hybrid VUV and TiO_2/UV processes. Sep. Purif. Technol. 54, 204–211.
Yang, W., Lu, Y., Zheng, F., Xue, X., Li, N., Liu, D., 2012. Adsorption behavior and mechanisms of norfloxacin onto porous resins and carbon nanotube. Chem. Eng. J. 179, 112–118.
Yean, S., Cong, L., Yavuz, C.T., Mayo, J.T., Yu, W.W., Kan, A.T., Colvin, V.L., Tomson, M.B., 2005. Effect of magnetite particle size on adsorption and desorption of arsenite and arsenate. J. Mater. Res. 20, 3255–3264.
Yu, X., Zhang, L., Liang, M., Sun, W., 2015. pH-dependent sulfonamides adsorption by carbon nanotubes with different surface oxygen contents. Chem. Eng. J. 279, 363–371.
Zhang, L., Song, X., Liu, X., Yang, L., Pan, F., Lv, J., 2011. Studies on the removal of tetracycline by multi-walled carbon nanotubes. Chem. Eng. J. 178, 26–33.
Zhang, Y., Liu, C., Xu, B., Qi, F., Chu, W., 2016. Degradation of benzotriazole by a novel Fenton-like reaction with mesoporous Cu/MnO_2: combination of adsorption and catalysis oxidation. Appl. Catal. B Environ. 199, 447–457.
Zhao, H., Liu, X., Cao, Z., Zhan, Y., Shi, X., Yang, Y., Zhou, J., Xu, J., 2016. Adsorption behavior and mechanism of chloramphenicols, sulfonamides, and non-antibiotic pharmaceuticals on multi-walled carbon nanotubes. J. Hazard. Mater. 310, 235–245.
Zheng, Q., Durkin, D.P., Elenewski, J.E., Sun, Y., Banek, N.A., Hua, L., Chen, H., Wagner, M.J., Zhang, W., Shuai, D., 2016. Visible-light-responsive graphitic carbon nitride: rational design and photocatalytic applications for water treatment. Environ. Sci. Technol. 50, 12938–12948.
Zhou, S., Shao, Y., Gao, N., Deng, J., Tan, C., 2013. Equilibrium, kinetic, and thermodynamic studies on the adsorption of triclosan onto multi-walled carbon nanotubes. Clean - Soil, Air, Water 41, 539–547.
Zhu, S., Liu, Y. guo, Liu, S. bo, Zeng, G. ming, Jiang, L. hua, Tan, X. fei, Zhou, L., Zeng, W., Li, T. ting, Yang, C. ping, 2017. Adsorption of emerging contaminant metformin using graphene oxide. Chemosphere 179, 20–28.
Zhu, W., Sun, F., Goei, R., Zhou, Y., 2017. Facile fabrication of RGO-WO_3 composites for effective visible light photocatalytic degradation of sulfamethoxazole. Appl. Catal. B Environ. 207, 93–102.
Zhuo, N., Lan, Y., Yang, W., Yang, Z., Li, X., Zhou, X., Liu, Y., Shen, J., Zhang, X., 2017. Adsorption of three selected pharmaceuticals and personal care products (PPCPs) onto MIL-101(Cr)/natural polymer composite beads. Sep. Purif. Technol. 177, 272–280.
Zúñiga-Benítez, H., Aristizábal-Ciro, C., Peñuela, G.A., 2016. Heterogeneous photocatalytic degradation of the endocrine-disrupting chemical Benzophenone-3: parameters optimization and by-products identification. J. Environ. Manag. 167, 246–258.